

Article

Impacts of Climate Change on Permafrost and Hydrological Processes in Northeast China

Wei Shan ^{1,2,3,4,*} , Yan Wang ¹ , Ying Guo ^{1,2,3,4}, Chengcheng Zhang ^{1,2,3,4}, Shuai Liu ¹  and Lisha Qiu ¹

- ¹ Institute of Cold Regions Science and Engineering, Northeast Forestry University, Harbin 150040, China
² Ministry of Education Observation and Research Station of Permafrost Geo-Environment System in Northeast China (MEORS-PGSNEC), Harbin 150040, China
³ Collaborative Innovation Centre for Permafrost Environment and Road Construction and Maintenance in Northeast China (CIC-PERCM), Harbin 150040, China
⁴ Low-Carbon Road Construction and Maintenance Engineering Technology Research Center in Northeast Permafrost Region of Heilongjiang Province (LCRCMET-HLJ), Harbin 150040, China
* Correspondence: shanwei@nefu.edu.cn

Abstract: Permafrost is very sensitive to climate change, and the accelerated degradation of permafrost in Northeast China caused by global climate change will change the hydrological and ecological processes in the region and cause significant impacts on natural systems and human activities. In this study, the spatial distribution of permafrost in Northeast China from 2000 to 2020 was simulated using an improved ground freezing number model. The spatial and temporal variations of permafrost thickness and active layer thickness were estimated using the mean ground temperature method based on the obtained permafrost distribution. Based on the above simulation results, the mean annual ground temperature and field monitoring temperature gradient, based on remote sensing estimation and the ice content data of permafrost, were used to calculate the amount of permafrost ice storage in Northeast China for many years and to predict the amount of water released from permafrost in the future to better reveal the influence of permafrost changes on ecohydrological changes in the watershed. The results show that, in the past 20 years, climate warming has led to the degradation of the permafrost area in Northeast China from $3.31 \times 10^5 \text{ km}^2$ to $2.70 \times 10^5 \text{ km}^2$, with a degradation rate of 18.43%; the stored ice in the permafrost has been released at an accelerated rate. The total ice storage volume in the permafrost of Northeast China is $3.178 \times 10^{11} \text{ m}^3$. The amount of ice storage in the permafrost increases with latitude and altitude, and the ice storage volume decreases to $6.641 \times 10^{10} \text{ m}^3$ after 100 years, which is a decrease of $2.514 \times 10^{11} \text{ m}^3$. The amount of water released due to permafrost degradation accounts for 79.11% of the current total ice storage, and the rate of water release reaches $2.51 \times 10^9 \text{ m}^3/\text{a}$. The release of water from permafrost has an important impact on river runoff whose source is at high altitudes, such as the Greater and Lesser Khingan Mountains in Northeast China.

Keywords: climate change; permafrost ice storage capacity; water released from permafrost; runoff



check for updates

Citation: Shan, W.; Wang, Y.; Guo, Y.; Zhang, C.; Liu, S.; Qiu, L. Impacts of Climate Change on Permafrost and Hydrological Processes in Northeast China. *Sustainability* **2023**, *15*, 4974. <https://doi.org/10.3390/su15064974>

Academic Editors: Francisca C. Aguiar and Rui Rivaes

Received: 12 February 2023

Revised: 3 March 2023

Accepted: 8 March 2023

Published: 10 March 2023



Copyright: © 2023 by the authors. Licensee MDPI, Basel, Switzerland. This article is an open access article distributed under the terms and conditions of the Creative Commons Attribution (CC BY) license (<https://creativecommons.org/licenses/by/4.0/>).

1. Introduction

Permafrost is a product of the comprehensive action of the atmosphere and the lithosphere, which is frozen and extremely sensitive to temperature changes [1]. Subsurface ice present in permafrost exists in the form of ice crystals or ice clay layers, where ice crystals can be as small as the nanometer level, and ice-bearing soil layers, which are relatively thick, are up to hundreds of meters thick in some areas [2]. Permafrost is an important component of high-latitude cold ecosystems, and the distribution pattern of permafrost in Northeast China mainly includes large discontinuous permafrost, island permafrost and sparse island permafrost [3]. Permafrost is usually considered an aquiclude [4], and its changes can directly lead to changes in water cycle processes [5]. The generation, infiltration and evapotranspiration of runoff in cold regions are always accompanied by the exchange of

water and heat during the freeze–thaw of the soil, which is a central aspect of the study of the water cycle in cold regions [6]. In the last 20a, the permafrost environment in Northeast China has changed significantly in response to climate warming, with the deepening of the active layer, reduction in permafrost area, a northward shift in the southern boundary and the expansion of the thawed area [4], and the rate of surface warming is significantly higher than the rate of global surface ground temperature increases reported in the IPCC Fifth Assessment of Climate Change [7,8]. Quantitative analysis of permafrost processes to predict future changes in permafrost is the key to permafrost research, and the response of ecosystems to permafrost degradation as it occurs is an important research component to reveal the relationship between permafrost and ecosystems.

The permafrost layer below the active layer is the key to maintaining the ecological environment of permafrost regions [9]. The large distribution of permafrost areas often has huge total subsurface ice reserves, and the huge amount of water released from permafrost degradation caused by global warming can further trigger ecohydrological effects, which have attracted widespread attention from scientists at home and abroad [10–12]. The potential contribution of permafrost thawing to increased river flow depends on the area of permafrost being thawed and the water content in the permafrost [13]. The study of permafrost distribution has become refined with the rise in computer and electronic information technology. Since the 1980s, mapping methods and models based on GIS technology have begun to be established [14–16]. Permafrost mapping tends to be large-scale, diversified and multifaceted in its presentation [17]. Most permafrost spatial distribution models are constructed based on actual measured permafrost data or remote sensing image data, and GIS technology is used to assign spatial characteristics to the data to display and express the spatial distribution of permafrost in the region. These permafrost models can be divided into empirical statistical models and physical models based on the actual energy balance process of permafrost [18]. The ‘Elevation Model’, one of the earliest empirical statistical models in China, classifies and divides permafrost according to the lower boundary of permafrost distribution and the relationship between the elevations [19–21]. Although it can simply classify permafrost [22], this method relies on DEM data. In addition, the classification of permafrost is only for a certain moment in time, and it cannot be dynamically discriminated. The mean annual ground temperature method refers to the use of the value of ground temperature that remains constant over a long time, almost unaffected by surface temperature fluctuations due to a certain depth, as a method of determining the presence or absence of permafrost [23,24]. It infers the state of permafrost in the region by obtaining the annual average ground temperature value for each point in the study area as the basis [25]. Nelson proposed the freezing index model in 1987, which simulates the distribution area of permafrost by calculating the surface freeze–thaw index [15] and has good application in high-latitude permafrost areas. Based on Stefan’s formula, Nan added the adjustment factor E to the original model and proposed an extended freezing index model to determine the presence or absence of permafrost based on the ratio of the freeze–thaw index F [26]. Nelson’s formula is only a special case, when $E = 1$. Nan, Feng, Bai et al. applied the improved freezing number model to the simulation of permafrost distribution on the Qinghai–Tibet Plateau and showed better simulation results. Compared with the multi-year permafrost maps made by previous researchers, it proved the applicability of the freezing number model in high-altitude permafrost regions, and multi-dimensional improvement space was also proved [26–28]. Lv et al. used the freezing number model to simulate the distribution of permafrost in the northeast region and proved that the freezing number model has good applicability in simulating the distribution of permafrost in the northeast region [29]. Shan [30] considered the influence of the vegetation canopy on satellite surface temperature data and used an improved freezing number model considering forest depression to better simulate the permafrost distribution in the permafrost region of Northeast China, providing a basis for more reasonable permafrost zoning in Northeast China. This was combined with field observation data to verify and make the first permafrost distribution map in Northeast China (Figure 1).

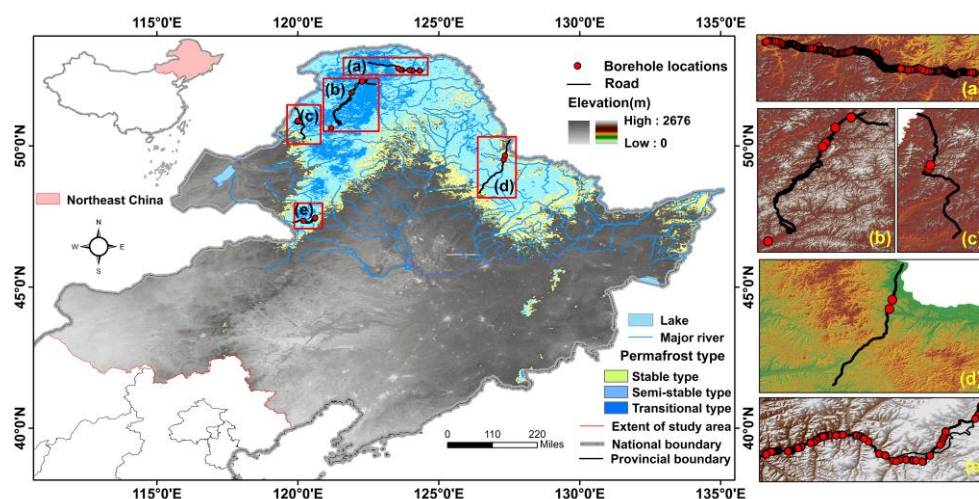


Figure 1. Distribution of elevation, permafrost and rivers in Northeast China, the distribution of elevation along the selected road located in the permafrost regions, and the distribution of borehole locations along the road are as follows from north to south: (a) Beijing–Mohe National Highway (G111); (b) Mangui–Genhe Provincial Highway (S204); (c) Shiwei–Labudalin Road (S201); (d) Bei’an–Heihe Expressway; (e) Ilshi–Chaiqiao Provincial Highway in Arxan (S308).

Studies on the calculation of water release from permafrost are often based on the spatial distribution data of permafrost combined with ice and water content in permafrost. Most studies of subsurface ice are based on the accretion and degradation of permafrost over many years, using field surveys, remote sensing techniques and laboratory analysis to estimate the distribution of subsurface ice, combined with statistical methods to calculate subsurface ice storage. Frampton et al. simulated near-surface flow in a permafrost system by using a non-isothermal and three-phase model and found that, due to the degradation of permafrost increasing the retention time and flow paths of subsurface runoff, the seasonal variability of runoff is lower, and they emphasized that hydrological data are relatively more accessible. Therefore, simulation studies from hydrological data are more likely to reflect perennial permafrost changes on long time scales compared to direct observations of permafrost [31]. Jeannine-Marie analyzed the long time series of flow from 23 hydrological stations located in the Northwest Territories of Canada and indicated that the melting of permafrost may lead to a significant trend of increases in winter baseflow and mean annual runoff of rivers in the permafrost region [11]. S. W. Lyon estimated that permafrost thickness in the Abiskojokken Basin in the subarctic circle of northern Sweden has decreased at a rate of 0.9 cm/a over the past 90 years based on receding water analysis. Then, the measured data and runoff characteristics from the hydrographic stations were used to explore the relationship between permafrost degradation and runoff at different warming rates [32], confirming the good applicability of the hydrological decline analysis method in analyzing permafrost melting and its rate [32]. With the continuous development of numerical simulation software, the role of hydrological models as an effective tool for studying runoff processes has become increasingly significant in the field of hydrology [33]. Mc Clelland et al. simulated the effect of permafrost thaw on river runoff in permafrost basins under different scenarios and found that permafrost thaw has caused an increase in annual runoff in major rivers originating in the Arctic permafrost region [13]. Evan applied the Sutra program to simulate groundwater in a river basin called Huliangou, which originates in the Qilian Mountains of China, and found that the contribution of groundwater to runoff increases threefold when the temperature increases by 2 °C [34]. Walwoord and Striegl et al. found that the degradation of permafrost increases baseflow [4]. Qin et al. found that the degradation of permafrost is one of the main causes of increased baseflow in the Qilian Mountains [35]. Connon and Duan et al. found that the melting of ice in permafrost and increased surface hydraulic connections after the

degradation of permafrost can also increase surface runoff [5,34]. Studies on permafrost water release frequently include data on the geographic distribution of permafrost along with calculations of the ice and water content in permafrost. Because permafrost areas are usually in high-altitude cold regions or subpolar regions where human activities are rare, the difficulty of arranging and implementing field experiments and the lack of data acquisition lead to a great limitation in understanding permafrost hydrological processes [34]. The SWAT model, an open-source hydrologic model, can be integrated with a variety of GIS software to simulate different aspects of hydrologic physicochemical processes using spatial information provided by remote sensing imagery and has been widely used both domestically and internationally [36–38] for areas where field data are scarce and long time series field survey data are difficult to obtain in harsh climatic environments [33]. Wang evaluated the performance of the snowmelt hydrology module of the SWAT model by simulating streamflow in the Wild Rice River Basin in northwestern Minnesota, and the results showed that SWAT can accurately simulate annual and monthly runoff as well as daily runoff from snowmelt in spring [39]. Two key components of excess soil moisture movement in permafrost and soil erosion prediction under snowpack were modified in the use of the SWAT model and improved the simulation of spring and winter baseflow [40]. Meng Xianyong [41] and Wang Shucai [33] used the SWAT model for river basins existing in the permafrost region, such as the Black River Basin in the Qilian Mountains of China and the Hulan River Basin located in the central part of Heilongjiang Province, respectively, and they verified that the SWAT model has practicality in the permafrost region, can be further improved according to the environmental conditions and can be well applied to the simulation of runoff processes in the permafrost region. Most studies on ecohydrological effects caused by permafrost water release in China are focused on the Qinghai-Tibet Plateau, which is due to the late start of permafrost research in Northeast China and the lack of ground observation data [42]. Few existing studies have concerned the hydrological effects of permafrost degradation in Northeast China, and it has not been determined how strong the direct effects of permafrost degradation in Northeast China are on the runoff yield and concentration due to the lack of a mechanistic model to quantitatively describe the effects of permafrost degradation on runoff as well.

Based on MODIS surface temperature and multi-source remote sensing geographic information data, combined with field monitoring data, this study considers the influence of plant canopies on the results of the satellite monitoring of surface temperature, and it simulates the distribution of permafrost in Northeast China using an improved freezing number model. The thickness distribution of permafrost in recent years was calculated based on the annual mean ground temperature method using field monitoring data of the annual mean ground temperature. The spatial distribution of ice storage in the permafrost region of Northeast China was obtained by counting the soil ice content data obtained from thousands of boreholes in the study area, extracting the ice storage volume and each layer separately using the point data of elevation and latitude, estimating the ice storage volume under current conditions, and predicting the water release volume and water release rate of permafrost in Northeast China under future scenarios. The SWAT model was used to simulate hydrological processes in the selected watersheds in the study area and to analyze the impact of permafrost on river runoff in the study area, providing a scientific reference for the study of permafrost changes and hydrological and ecological responses.

2. Materials and Methods

2.1. Study Area

Northeast China (38°72′–53°56′ N, 115°52′–135°09′ E) [43] includes Heilongjiang, Jilin, Liaoning and the five eastern leagues of the Inner Mongolia Autonomous Region (Hulunbeier, Xing'an, Tongliao, Chifeng and Xilingol) (Figure 1), with a total area of about $142 \times 104 \text{ km}^2$, which is the second largest permafrost region in China [44]. According to the geographical and climatic conditions affecting the spatial distribution of permafrost, the northeast permafrost region can be divided into the discontinuous permafrost region, island

permafrost region and sparse island permafrost region. The terrain can be clearly divided into mountains, plains, woodlands and plateaus and is surrounded by mountains on three sides and plains in the interior, which can be divided into the Songnun Plain, Sanjiang Plain, Liaohe Plain, Greater Khingan, Lesser Khingan and Changbai Mountains [45]. Covered with extensive forests along with some bogs and peat layers, these luxuriant forests and mossy peat layers attenuate solar radiation and provide environmental support for the development and maintenance of permafrost. The northeast region has a cold-temperate continental monsoon climate with four distinct seasons and simultaneous rain and heat [46]. As the temperature decreases in winter, soil freezing and the snow line occur in Northeast China, changing the regional runoff yield and concentration process; when the temperature rises in spring, it is accompanied by the melting of snow and ice in permafrost. The snowmelt runoff and loamy midstream flow are formed to recharge the river runoff, and the runoff yield and concentration mechanism of the watershed in Northeast China have the characteristics of a cold region runoff yield and concentration.

The distribution of major river basins in the northeast permafrost region is shown in Figure 2. The hydrological area in the northern part of the Greater Khingan Mountains mainly includes the Jiliu River Basin, the Eimur River Basin, the Pangu River Basin and the Huma River Basin, which are radially shaped and injected into the Heilongjiang River. There is permafrost under the ground, and the groundwater is relatively abundant, mostly pressurized and then spontaneously gushing out. Moreover, the upper reaches of the rivers have large vegetation coverage, which is conducive to the adjustment of runoff. Spring flooding comes in late April to early May, and river ice begins to melt. Spring flooding generally lasts more than 40 days, and the annual flooding of river water, due to differences in the amount of snow, accounts for about 20% of the total annual river runoff. Usually in the spring ice meltwater is not completely drained, the rainy season has come, followed by the summer floods. Therefore, spring and summer floods are connected. Sometimes, a runoff decline period appears between the two floods, but the runoff is more gentle. In mid to late August, the region enters a period when the river is at its normal level, and the river water from June to September accounts for 60–80% of the annual water. The maximum runoff and the annual maximum volume of water are reached more often in July. The river freezes in late October, and the thawing layer of the soil is frozen successively in the season. The river enters the dry season in winter, which continues until April of the next year. The river ice thaws in the first ten days of May, and the freezing period lasts more than half a year. The river network in the eastern hydrological region of the Greater Khingan Mountains is dense, and the river flow direction is formed from northwest to southeast due to the elevation difference of the mountains. The main rivers distributed in the region are the Nenjiang River and its tributaries, such as the Genhe River, Nuomin River, Taoer River, etc. As the temperature is higher than that in the north, evaporation is enhanced, and the annual average runoff depth is 50–200 mm. Spring flooding comes a little earlier than it does in the north. It generally lasts 35–50 days from the first ten days of April to the middle and the last ten days of May. Generally, due to the relatively small amount of snow, the spring flood water volume is lower, accounting for only 5–20% of the annual water volume. The summer flood season in this region occurs from late June or early July to early October. Compared with the northern region, it occurs about one month later, and it takes 90–130 days. Summer flood water accounts for 60–80% of the annual river runoff. The dry season of autumn and winter begins in middle and late October, and the river is generally in the winter freezing period from late October or early November to middle and late April, with a total length of 120–170 days.

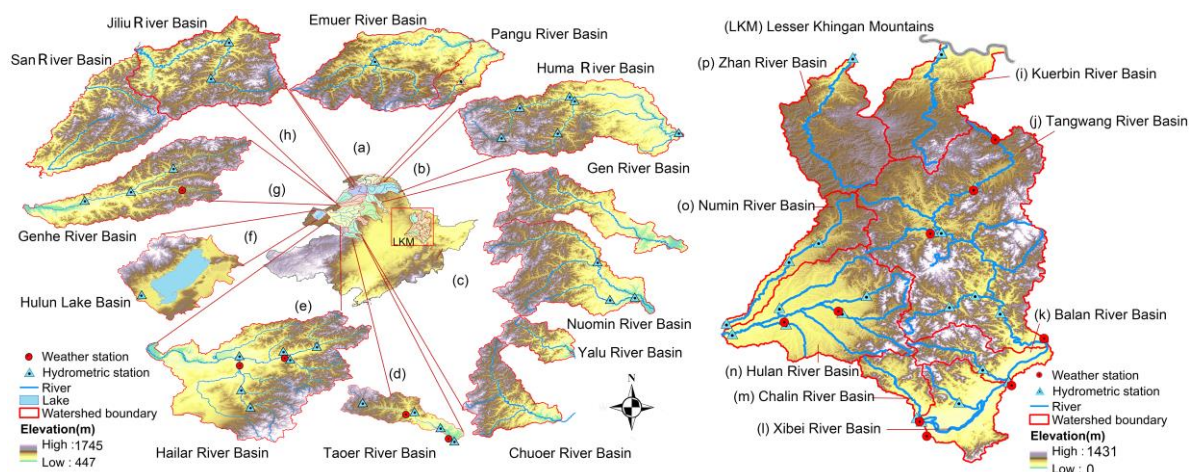


Figure 2. Watersheds where the simulated lakes and rivers are located, and the location of hydrological and meteorological stations. The Greater Khingan Mountains region is divided into (a) the basins of the Emuer and Pangu rivers, (b) the basin of the Huma river, (c) the basin of the Nuomin river, (d) the basin of the Taoyer river, (e) the basin of the Hailar river, (f) the basin of the Hulun lake, (g) the basin of the Gen river and (h) the basin of the Jiliu river. (Lesser Khingan Mountains, abbreviated as LKM) Lesser Khingan Mountains region is divided into the (i) Kuerbin River Basin, (j) Tangwang River Basin, (k) Balan River Basin, (l) Xibei River Basin, (m) Chalin River Basin, (n) Hulan River Basin, (o) Nuomin River Basin and (p) Zhan River Basin in this study.

The rivers in the permafrost regions of the Lesser Khingan Mountains include the Northwest River, Chalin River, Hulan River, Tangwang River, Balan River, Numin River, Zhanhe River (a tributary of the Sun River) and the Kuerbin River (a tributary of the southern bank of the middle reaches of Heilongjiang Province), and the distribution of each river basin is shown in Figure 2. The vegetation coverage in the study area of the Lesser Khingan Mountains watershed is more than 70%. High vegetation coverage is conducive to the storage of frozen soil and has a good regulating effect on river runoff. The annual distribution of runoff in the study basin is uneven. The maximum runoff occurs in June and July, and the snowmelt runoff accounts for a large proportion. This is due to the influence of climate, vegetation, topography, geomorphology, hydrology and other aspects by which the permafrost in Northeast China is developed and maintained.

2.2. Data Sources

The remote sensing data include Digital Elevation Model (DEM) data from the NASA Shuttle Radar Topography Mission (SRTM) with a resolution of 30 m and projected coordinates of WGS84 (<http://www.resdc.cn/data.aspx?dataid=217>, accessed on 6 April 2022). Water vapor pressure (Ewp) data were obtained from the WorldClim v. 2.1 release of global terrestrial 1 km spatial resolution climate data in kilopascals in the geographic coordinate system WGS84 (accessed on: <https://www.worldclim.org/data/worldclim21.html>, accessed on 22 November 2022). The surface temperatures (LST) are from NASA's Land Processes Distributed Active Archive Center (LP DAAC/NASA), obtained by processing the MODIS dataset MOD11A2. The time range is from 2000 to 2020, the temporal resolutions are 8 days and monthly, and the spatial resolution is 1 km (<https://lpdaac.usgs.gov/>, accessed on 22 November 2022). Because the MODIS data cover the period from March 2000 to the present, the data for January and February 2000 are supplemented by the average of the data for January–February 2001 and 2002. Soil moisture content data (ω) are derived from the soil moisture content data in the ERA5-LAND reanalysis dataset provided by the European Centre For Medium-Range Weather Forecasts (ECWMF) with a spatial resolution of 0.1×0.1 degrees (ERA5-Land monthly averaged data from 1950 to present <https://cds.climate.copernicus.eu/cdsapp#!/dataset/10.24381/cds.68d2bb30?tab=overview>, accessed on 3 September 2022). Surface air temperature (T_a) was obtained from the Na-

tional Science and Technology Infrastructure Platform-National Center for Earth System Science and Data with a spatial resolution of 1 km and a time range of 2000–2020 (<http://www.geodata.cn>, accessed on 20 August 2022).

Data on soil types, properties and spatial distributions in the study area were obtained from the Harmonized World Soil Database v1.2 (hereinafter referred to as HWSD) published by the Food and Agriculture Organization of the United Nations (FAO) at a resolution of 1 km (http://webarchive.iiasa.ac.at/Research/LUC/External-World-soil-database/HTML/HWSD_Data.html?sb=4, accessed on 20 September 2022). The land use data were based on the spatial distribution data of the remote sensing monitoring of land use types nationwide (<http://www.resdc.cn/Datalist1.aspx?FieldTyepID=1,3>, accessed on 20 September 2022), published by the Institute of Geographical Sciences and Resources of the Chinese Academy of Sciences. The data were generated via manual visual interpretations of Landsat TM imagery with a resolution of 1 km. The data on hydrological elements, such as river runoff, in the study area were obtained from the Geographic Remote Sensing Ecological Network (<http://www.gisrs.cn/>, accessed on 26 April 2022) and the China Water and Rainfall Information Network (<http://xxfb.mwr.cn/>, accessed on 2 March 2022), and the actual data of hydrological stations released by the China Hydrological Yearbook mainly included precipitation, runoff, evaporation and temperature. The geothermal monitoring data were obtained from the survey reports of the Valagan-Xilinji G111 and Alshan S308 highway of the Jing-Mo Expressway and the Field Scientific Observation and Research Station of the Ministry of Education—Northeast Permafrost Region Geological Environment System (FSSE-PFNEC). The locations of the monitoring points are shown in Figure 1. The measurement period is 2016–2020, and the measurement depth is 4–19 m.

2.3. Methods

2.3.1. Analysis of Area Change of Permafrost

Permafrost in Northeast China is an important part of permafrost at high latitudes in China, and the existence of permafrost plays an important role in maintaining the climate and ecology of permafrost areas and even globally, especially its hydrological significance. Therefore, studying the change in permafrost regions has some scientific value in analyzing its hydrological role. Equation (1) uses a modular freezing number model to simulate the distribution of perennial permafrost at high latitudes in China, where DDF and DDT are the surface freezing index and melting index ($^{\circ}\text{C}\cdot\text{day}$) [26]. The surface freezing index, also known as the negative surface temperature, is the sum of the daily average ground temperatures below 0°C during the freezing period; the surface thawing index, also known as the positive surface temperature, is the cumulative daily average ground temperature above 0°C during the thawing period. The freezing index model proposed by Nelson can further calculate the thawing index (DDT) and the freezing index (DDF) by approximating the surface temperature as a periodic cosine function. The calculation equations are Equations (2) and (3), respectively [27,28]. The E factor, characterizing the soil conditions in the freezing index method, is improved according to the soil conditions in Northeast China. The E factor depends on the freeze–thaw properties of the soil and characterizes the parameters affecting the formation, development and preservation of permafrost, and it is dimensionless. In this paper, an improved method for calculating the E factor is formed by linking the model for calculating the thermal conductivity of frozen soil [47,48] and the model for calculating the thermal conductivity of thawed soil [47,49,50] with the calculation of the E factor by referring to the previous test models and test results, and the calculation procedure is shown in Equation (4). The changing pattern of permafrost distribution area in Northeast China in the past 20 years is analyzed.

$$F = \frac{\sqrt{\text{DDF}}}{\sqrt{\text{DDF} + E \times \sqrt{\text{DDT}}}} \quad (1)$$

$$DDT = (T_a + A \left(\frac{\sin(\cos^{-1}(-\frac{T_a}{A}))}{\cos^{-1}(-\frac{T_a}{A})} \right)) \times (365 \times \frac{\cos^{-1}(-\frac{T_a}{A})}{\pi}) \quad (2)$$

$$DDF = -(T_a - A \left(\frac{\sin(\cos^{-1}(-\frac{T_a}{A}))}{\pi - \cos^{-1}(-\frac{T_a}{A})} \right)) \times (365 - 365 \times \frac{\cos^{-1}(-\frac{T_a}{A})}{\pi}) \quad (3)$$

where T_a is the annual mean surface 0 cm temperature ($^{\circ}\text{C}$), and A is the annual surface temperature amplitude ($^{\circ}\text{C}$).

$$E = \sqrt{\frac{0.1442(0.7 \log \omega_t + 0.4) \times 10^{0.6243\rho_s} \times L \times \rho_s(\omega_f - \omega_u)}{0.8525 - 0.0125(T_0 - T_a) + 1.3787(0.1298 \ln(10 \times E_{wp}) + 0.0495) \times L \times \rho_s(\omega_t - \omega_u)}} \quad (4)$$

where ρ_s is the dry density of the soil (kg/m^3), ω_t and ω_f are the total water content of the soil during the thawing and freezing periods, respectively (%), ω_u is the unfrozen water content of the soil (%), E_{wp} is the water vapor pressure (kPa), T_0 is the surface temperature, and T_a is the air temperature. Except for L ($3.352 \times 10^5 \text{ J}\cdot\text{kg}^{-1}$), the latent heat of melting per unit of mass of ice, which is taken as a constant value, the raster distribution data of the variables in Northeast China are used in the calculation.

In the process of the above calculation, the daily average annual ground temperature of Northeast China was obtained by processing the MODIS data product (MODIS/006/MOD11A1) using the Google Earth Engine (hereinafter referred to as GEE) for Northeast China. In the permafrost region of the northeast, the surface temperature is above zero from mid-April to mid-October every year. Because the temperature transfer and freezing process in the soil has a lag, the period from May to October is set as the soil thawing period, and the period from November to April is set as the soil freezing period. The soil water content data in the ERA5-LAND reanalysis dataset were extracted via the GEE for different periods year by year to obtain the annual soil thawing period water content (ω_t) and freezing periods (ω_f). To unify the resolution, the grid data were resampled to a 1 km resolution in ArcGIS using the NEAREST resampling method and then by using grid calculation. For the value of the soil dry density (denoted by ρ_s), most of the previous authors used the density of several types of soils in the study area, which accounted for the largest proportion of the total area, and they then used the calculation as the overall soil density value of the study area after proportional conversion. In this study, the ρ_s value is taken from the dry bulk density (REF_BULK_DENSITY) of soil in the database corresponding to the soil distributed in Northeast China in the World Soil Database, and then calculations are made after grid reassignment. The unfrozen water content (denoted by ω_u) is calculated from the distribution data of Northeast China soils from the World Soil Database, combined with the SPAW model developed by Washington State University to obtain the soil wet density (denoted by ρ_w) [33], and after unit conversion, the distribution data of the soil water content in Northeast China are calculated using Equation (5) as the unfrozen water content value (ω_u) to use in the calculation. The unfrozen water content of rivers, lakes and other water bodies is assigned a value of 1 because water bodies are not numbered and classified in the Chinese soil database.

$$\omega_u = \rho_w - \rho_s \quad (5)$$

Because the surface temperature detected by the satellite sensor is affected by plant canopies in densely vegetated areas, resulting in deviations between the satellite-measured surface temperature and the actual surface temperature, the freezing number vegetation factor influence is calculated using Equation (6), proposed by Shan [43], which takes into account the influence of vegetation and is used for year-by-year correction.

$$Fnc = \varepsilon_{fcc}[(MANDVI_G)_t + 1] \times Fn \quad (6)$$

where ε_{fcc} is the canopy closure, averaged over the study area between 0.2 and 0.69, with a constant value of 0.56 according to Shan [43] in a study of permafrost distribution in Northeast China. $MANDVI_G$ is the mean value of NDVI for each growing season, representing the overall state of vegetation coverage during the year. t is the time period ($t = 2000, 2001, \dots, 2020$).

2.3.2. Thickness Analysis of Permafrost

The mean annual ground temperature (MAGT) method was used to zone the permafrost in Northeast China. Because the surface vegetation coverage in the permafrost region in Northeast China is large, the effect of plant canopies and forest canopy closure was considered. Therefore, Equation (7) is used after using to Equation (6), and the MAGT is corrected based on the measured ground temperature data from the drilling.

$$MAGT_r = a \times \varepsilon_{fcc} \times NDVI + MAGT \quad (7)$$

where $MAGT_r$ is the corrected annual average surface temperature, and a is the correction coefficient, adjusted according to the measured ground temperature data from the drilling and the value of the freezing number at the corresponding sites calculated above, taking the value $a = 9.8$ to use in the calculation. The value of the forest canopy closure (ε_{fcc}) is taken as a constant value of 0.56, with reference to the study of Shan et al. above on the distribution of permafrost in the northeast [43].

The thickness of permafrost is calculated based on the one-dimensional equation of heat conduction, and the relationship between the thickness of permafrost and the average annual ground temperature can be expressed using Equation (8) [1].

$$h_t = -T_{cp} \frac{\lambda}{q} + h \quad (8)$$

where h_t is the thickness of permafrost (m), T_{cp} is the annual average ground temperature over the whole surface, q is the terrestrial heat flow, $q = g\lambda$, g is the geothermal gradient, λ is the thermal conductivity, h is the annual depth of geothermal variation, and h is taken as a constant value of 11 m from the field survey data of Chang in the Greater Khingan Mountains region [51]. The ground temperature gradient g is calculated from the data of a 1–19 m depth borehole survey from 18 to 22 years to take a value of 0.061 °C/m.

2.3.3. Estimation of Ice Content in Permafrost

As an example, a total of 1122 field boreholes were reported during the survey and design process of the Beijing–Mohe National Highway, and the subsurface ice distribution and distribution characteristics of the borehole profiles were analyzed after careful screening. According to the distribution characteristics of underground ice in the horizontal direction, the permafrost along the Beijing–Mohe National Highway is divided into five categories: less frozen soil, more ice and frozen soil, rich ice and frozen soil, full ice and frozen soil, and a soil-bearing ice layer. The first two are collectively referred to as low ice-bearing permafrost, and the last three are referred to as high ice-bearing permafrost [22]. The mileage of each type of permafrost along the road was also counted in detail. Each borehole was divided into three depth sections in the vertical direction: within the range of 1–5 m below the upper limit of permafrost, 5–10 m deep below the upper limit and 10 m below the upper limit, and the subsurface ice reserves at each depth were counted. The ice content of permafrost in the region is estimated using Equation (9) [27,52].

$$W = \frac{Ah_t\gamma_d}{\rho} W_i \quad (9)$$

where W is the total ice content under permafrost (m³), A is the area of permafrost (m²), h_t is the thickness of permafrost (m), γ_d is the dry bulk density of soil (kg/m³), ρ is the density of ice (kg/m³), and W_i is the ice content of layer i after removing unfrozen water. The value

of W_i is taken with reference to data in the literature and the construction survey report of the Beijing–Mohe National Highway. The existence of a thawing interlayer was not considered in this study, and the ice content after removing unfrozen water in each layer was taken as the average value of each layer instead [53], which was taken as $W_1 = 16\%$, $W_2 = 12\%$ and $W_3 = 5\%$.

The calculated ice content of each layer was superimposed to obtain the spatial distribution of permafrost ice storage in the current scenario, and the total current subsurface ice storage in the permafrost region of Northeast China was estimated based on this. The freezing of the soil in Northeast China is influenced by latitude and elevation, so the ice storage volume of each layer was extracted separately using the point data of elevation and latitude. The sum of the ice content every 200 m in elevation and every degree in latitude was calculated, and the variation in ice storage volume with latitude and elevation in Northeast China was analyzed in the current situation.

2.3.4. Hydrological Simulation of River Basins in Permafrost Regions of Northeast China

By establishing the distributed hydrological models of twelve river basins with river sources in the Greater Khingan Mountains and the watersheds of the 8 rivers with their sources in the Lesser Khingan Mountains, as well as the Hulun Lake Basin, which is situated on a grassland, meteorological and soil data sequences were established and substituted into the SWAT model with the support of GIS technology. The correlation between runoff changes and permafrost in Northeast China was investigated based on the SWAT model simulating runoff changes in watersheds under different permafrost conditions, providing a reliable basis for water resource allocation and hydrological studies in the permafrost region of Northeast China. The SWAT model requires that all spatial data have the same spatial reference and geographic coordinate system to ensure that the same geographic location is in the same pixel [33]. The projection coordinate system used in this paper is Albers' equiprojected conic projection, and the geographic coordinate system is WGS_84. The runoff rate is determined by using the measured data from hydrological and meteorological stations. The calibration period is 2000–2001, and the validation period is 2003–2020. The distribution of rivers and hydrological and meteorological stations in the basin, as well as the basin, is shown in Figure 2. The ordinary kriging method was used to interpolate the data from hydrological and rainfall stations in each watershed to calculate the precipitation in each watershed.

Based on the summary analysis of vegetation, soil types and basin meteorological and hydrological data of the selected watersheds, the eco-hydrological processes in the permafrost region under different climatic conditions were simulated. The runoff curve number method-SCS-CN empirical model proposed by the United States Department of Agriculture Soil Conservation Service (USDA SCS) was adopted. The model structure is simple and requires only one comprehensive parameter: the runoff curve number (CN), which reflects the characteristics of the watershed subsurface before rainfall, and it is widely used in many countries and regions with the empirical relationship of Equations (10) and (11) [54].

$$Q_{\text{surf}} = (R_{\text{day}} - I_a)^2 / (R_{\text{day}} - I_a + S) \quad (10)$$

$$S = S_{\text{max}} \left(1 - \frac{S_w}{S_w + \exp(w_1 - w_2 S_w)} \right) \quad (11)$$

where R_{day} is the daily precipitation (mm); I_a is the initial loss, including sink filling, interception, etc. (mm); S is the interception, which can be calculated according to the soil water content (mm); S_{max} is the maximum daily interception (mm); S_w is the available amount of soil water (mm); and w_1 and w_2 are shape coefficients.

After previous experiments and research, this model can improve the surface runoff module of the SWAT model by combining the special substratum and climate conditions in the permafrost regions, and it can better invert the process of runoff simulation. The

improved model still has the advantages of a simple structure, fewer parameters and the ability to objectively describe the surface runoff process under different soil types and different precipitation conditions. In conditions in which the soil contains permafrost, Equation (12) can be used to correct the soil interception [55].

$$S_{\text{frz}} = S_{\text{max}}[1 - \exp(-0.000862S)] \quad (12)$$

where S_{frz} is the daily interception under the condition that the soil contains permafrost (mm).

In the SWAT model, when the soil temperature ≤ 0 is considered as the presence of permafrost, the interception S is replaced by S_{frz} . Because the value of S_{frz} is smaller, when the soil temperature is > 0 , the interception suddenly increases, resulting in a more significant decrease in surface runoff [56]. Soil freeze–thaw at high latitudes is a long-term process. Permafrost in the Greater Khingan Mountains starts to freeze in November of the calendar year, and the thawing starts in late March of the following year. Xiao et al. [57] considered soil thawing rate as a relative function of the time elapsed for soil thawing and verified it using measured data. Accordingly, in this paper, the soil freeze–thaw rate is considered as a function of soil temperature, and the calculation of the freeze–thaw period interception is based on the freeze–thaw rate, which is expressed in Equation (13).

$$S_v = S_{\text{frz}} + \left[1 - (1 - T_{\text{sol}}/T_t)^{0.8}\right](S - S_{\text{frz}}) \quad (13)$$

$T_{\text{sol}} \in [0, T_t]$

where S_v is the freeze–thaw interception (mm); T_{sol} is the soil temperature ($^{\circ}\text{C}$); and T_t is the freeze–thaw threshold ($^{\circ}\text{C}$) obtained using parameter rate determination. A value of 0.8 was selected with reference to the results of Xiao et al.

2.3.5. Accuracy Verification of Hydrological Model Simulation Results

Parameter calibration and sensitivity analysis were conducted on the simulation results of the SWAT model. The coefficient of determination (R^2) was selected, and the Nash–Sutcliffe coefficient (E_{ns}) was used to test the simulation effect of the model. The Nash–Sutcliffe coefficient (E_{ns}) can reflect the fitting of the simulated value and measured value, and its value range is generally 0~1. Only when $E_{\text{ns}} > 0.5$, the simulation result is acceptable. The coefficient of determination R^2 can reflect the coincidence between the simulated value and the measured value, and its value range is from 0 to 1. Only when R^2 is > 0.5 , the simulation result is considered acceptable. It is generally considered that the model simulation accuracy is satisfactory when R^2 is higher than 0.65 and E_{ns} is higher than 0.60, calculated using Equations (14) and (15) [58]. Finally, Pearson correlation analysis was applied to analyze the interaction mechanism between meteorological and hydrological factors.

$$E_{\text{ns}} = 1 - \frac{\sum_{i=1}^n (Q_s - P_m)^2}{\sum_{i=1}^n (Q_s - Q_p)^2} \quad (14)$$

$$R^2 = \frac{\left[\sum_{i=1}^n (Q_s - Q_p)(P_m - P_p)\right]^2}{\sum_{i=1}^n (Q_s - Q_p)^2 \sum_{i=1}^n (P_m - P_p)^2} \quad (15)$$

where Q_s is the actual measured value; P_m is the simulated value; Q_p is the average of measured values; and P_p is the simulated average.

3. Results

Patterns and Trends of Permafrost and Runoff in the Permafrost Regions of Northeast China

The temperature changes in the permafrost regions of Northeast China show an increasing trend, with a total increase of 0.65 °C from 2000 to 2020, and this trend has a strong persistence in the future, which is consistent with the global temperature tendency. The average number of precipitation days per year in the selected permafrost basins is 85 d. Precipitation is unevenly distributed within the year, with the maximum continuous precipitation occurring mostly in June–September, accounting for 66% of the annual precipitation. Precipitation on the eastern slope of the Great Khingan Mountains mainly comes from the western Pacific monsoon, and the interannual variation in precipitation is large, with a ratio of precipitation in the abundant to dry years at about 3.0. Most of the rivers have the same trend of interannual variation in runoff and temperature, with a correlation coefficient of 0.932 and a correlation coefficient of 0.909 between runoff and precipitation.

The calculation results show that the northern part of the western slope of the Great Khingan Mountains in Northeast China is bounded by the Erguna River and the Heilongjiang River. The southwestern part is along the line of Moldauga and Derbure to the south and to the east of the Tuli River, and along the eastern side of the ridge line of the Great Khingan Mountains to the Heilongjiang River to Mohe, there is an area of about 6.16×10^4 km² located in the northernmost part of China with a low average annual temperature of −4 °C or less. The high vegetation coverage in this area, as well as the rainy summer, sparse winter precipitation and light snow coverage conditions, is more conducive to ground heat dissipation and cooling, and it is also conducive to the preservation and development of the permafrost layer. This region has the lowest temperature and the largest thickness of permafrost in the regions of the Greater and Lesser Khingan Mountains. The density of ice content in Northeast China is between 0–8 m, and the density of ice content varies greatly from region to region. The freezing of the soil in Northeast China is greatly affected by latitude and altitude and is almost not affected by longitude. According to the elevation and latitude data of Northeast China, the ice content of permafrost varies greatly with the elevation. We expressed the ice content in the soil layer of each pixel by converting it into the thickness of the ice layer (m). In addition, we expressed the ice content by superimposing the ice content calculated for each pixel point in the study region within the set elevation range in units of 200 m in elevation, and we superimposed the ice content calculated for all pixels in the study region within the set unit latitude range in units of ° in latitude. The spatial distribution of ice reserves in Northeast China under the current scenario and the variation in ice reserves with latitude and elevation were obtained (Figure 3). We calculated the thickness of permafrost after 100 years based on the temperature rise rate of 0.04 °C/a. Figure 3e shows the spatial distribution of the ice content of permafrost after 100 years. Most of the permafrost in Northeast China is located in the Greater and Lesser Khingan Mountains, and because most of the regions in the Greater and Lesser Khingan Mountains are between 800 m and 1200 m in elevation, there are not many peaks with an altitude of more than 1400 m. However, the Changbai Mountains in the southeast coastal area of Northeast China are very high in elevation, and the highest peak elevation is the highest elevation in the entire northeast region. However, it accounts for a very small proportion of the area of Northeast China and is much smaller than the permafrost region of the Greater and Lesser Khingan Mountains, which makes ice storage in Northeast China reach a maximum at an elevation of 1000 m. In addition, the value of ice storage at an elevation above 1200 m gradually decreases. Figure 3g shows the elevation distribution in Northeast China, and two watersheds with different latitudes and large elevation changes were selected as examples to illustrate the spatial distribution of the present ice reserves in the Northeast China permafrost region and the predicted changes in 100 years. To better show the true latitudinal span of the shown watersheds on the Earth, the projection coordinates of Figure 3 were taken in the Krasovsky_1940_Albers projection mode, which takes into account the curvature of the Earth. It can be seen that, in the next 100 years, ice reserves in Northeast China will be significantly reduced, and

those at lower latitudes will degrade more rapidly than those at higher latitudes, with almost no permafrost remaining in the southern edge of the present tundra and with subsurface ice disappearing. The comparison between the Jiliu River Basin in Figure 3h and the Hailar River Basin in Figure 3i shows that the lower elevation areas degrade more rapidly than the higher elevation areas do. The ice storage in the same latitudinal range tends to decrease from the ridges to lower elevations. Many large rivers in Northeast China have thawed areas underneath them, where permafrost does not exist. Due to the special geological structure, there are volcanoes and underground hot springs in some places, and the river water temperature is relatively high. Therefore, future permafrost degradation spreads along the river toward both sides of the river, and the ice storage volume gradually decreases along the river toward both sides of the river.

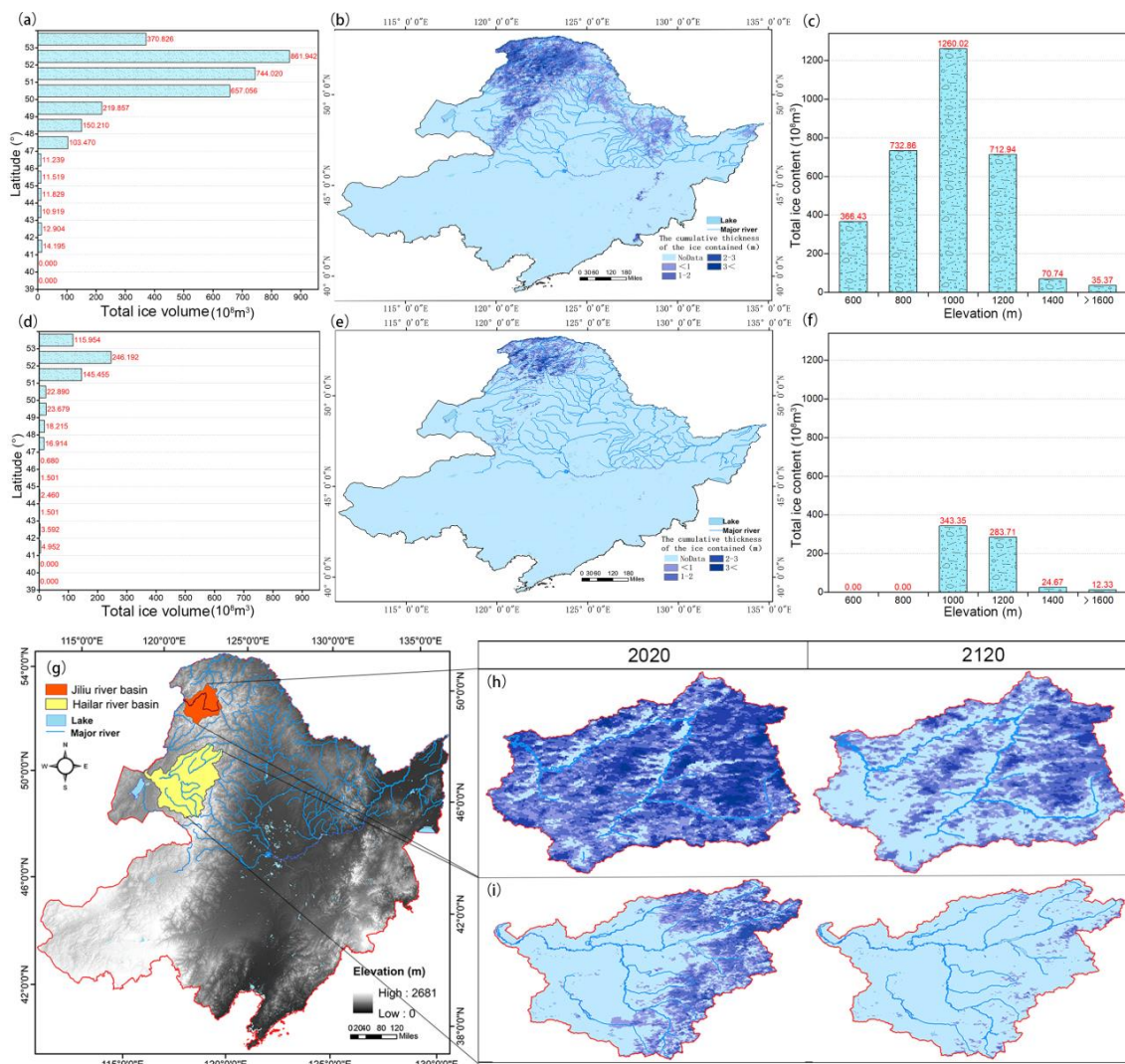


Figure 3. (a) At present, the latitude distribution of ice storage in northeast permafrost; (b) At present, the spatial distribution of the ice storage capacity of permafrost in Northeast China; (c) At present, the latitude distribution of ice storage in northeast permafrost; (d) Latitude distribution of ice storage in the permafrost of Northeast China after 100 years; (e) Spatial distribution of accumulated ice storage in northeast permafrost after 100 years; (f) Latitude distribution of ice storage in northeast permafrost after 100 years. Detailed presentations of different types of basins are as follows: (g) Location and elevation distribution of the presented basins; (h) Spatial distribution of ice reserves in the Jiliu River Basin at higher latitudes at present and after 100 years; (i) Spatial distribution of ice reserves in the Hailar River Basin at lower latitudes at present and after 100 years.

The accumulated ice storage in island permafrost areas and some areas at the edge of permafrost with low altitudes is generally small, most of which is below 2 m, mainly because of the small thickness of its permafrost. In areas with high altitudes, such as the mountains of the Greater and Lesser Khingan Mountains, the Changbai Mountains and other large areas of continuous permafrost, the average accumulated ice storage of permafrost is high. The runoff of river water is not only related to precipitation but also related to temperature, and temperature is positively correlated with the amount of water released by ice melting in the “active layer” above the permafrost. From late March, the temperature in the basins gradually stabilizes above 0 °C. The permafrost layer under the “active layer” starts to melt downward from the top, the thickness of the active layer becomes larger, and the phreatic water formed by the melting ice in the permafrost is recharged by the river through underground runoff, which increases river runoff. See Table 1 for the geo-environmental data, model simulation and parameter calibration results related to hydrology in each basin from 2000 to 2020. The partial correlation method in statistics was used to analyze the relationship between runoff change and climate and the thickness of the active layer. Through partial correlation analysis, the runoff change in the northeast permafrost region was determined to have a certain positive correlation with the temperature ($p = 0.755$, significance levels are expressed as α , $\alpha < 0.1$) and the thickness of the active layer ($p = 0.783$, $\alpha < 0.1$) for natural factors.

Table 1. Simulation and parameter calibration of the hydrological model of the studied basin from 2000 to 2020 and the hydrological environment of the basin.

Number	Watershed Name	Longitude and Latitude	Area (km ²)	Air Temp (°C)	Elevation (m)	Length (km)/Width (m)/Depth (m)	Annual Runoff (10 ⁸ m ³)
a	Emuer	122°21′ E~122°22′ E, 53°29′ N~53°27′ N	16,105.9	−4.4	246–1383	469/20~150/25	27.32
	Pangu	123°20′ E~124°35′ E, 52°22′ N~53°09′ N	3631.9	−4.4	236–1375	165/20~45/1.2	14.3
b	Huma	122°12′ E~126°43′ E, 51°17′ N~52°41′ N	31,196.1	−2.7	160–1518	524/50~200/1.2	67.51
c	Nuomin	122°12′ E~126°43′ E, 51°17′ N~52°41′ N	25,740.7	−1.2	165–1410	466/60~170/2.2	46.41
d	Taoer	120°10′ E~124°00′ E, 45°42′ N~47°15′ N	8414.1	4.5	253–1745	563/10~50/1.0	8.93
e	Hailaer	117°51′ E~122°27′ E, 47°33′ N~50°16′ N	50,446.9	−0.89	534–1710	622/50~200/1.2	37.81
f	Hulun	117°00′ E~117°42′ E, 48°30′ N~49°21′ N	2338.9	−0.24	447–1002	5.7 (Lake depth)	13.62 (max/min is 21.29)
g	Gen	119°23′ E~122°42′ E, 50°14′ N~51°13′ N	15,787.9	−4.6	512–1440	469/20~150/25	20.20
h	Jiliu	120°35′ E~122°50′ E, 51°02′ N~52°30′ N	15,771.7	−4.3	417–1512	165/20~45/1.2	42.31
i	Kuerbin	128°19′ E~129°31′ E 48°15′ N~49°26′ N	5826.2	−0.5	86–792	221/30~65/1.8	2.72
j	Tangwang	128°8′ E~129°54′ E 46°36′ N~48°44′ N	20,699.4	−1.7	174–798	523/90~130/3.0	55.20
k	Balan	128°36′ E~129°58′ E 46°19′ N~46°52′ N	2075.6	2.5	190–1029	108/20~60/0.7	5.55
l	Xibei	128°44′ E~129°34′ E 46°5′ N~46°28′ N	794.5	2.4	102–1121	74/15~28/1.1	15.21
m	Chalin	128°44′ E~129°54′ E 45°57′ N~46°34′ N	1191.8	2.5	196–1424	91/20~70/1.1	5.16
n	Hulan	128°8′ E~129°33′ E 46°36′ N~47°18′ N	9953.8	2.5	134–1350	523/90~130/3.0	42.29
o	Numin	126°55′ E~128°20′ E 46°50′ N~48°06′ N	3309.5	2.1	76–624	265/20~50/0.8	29.3
p	Zhan	127°27′ E~128°29′ E 48°02′ N~49°21′ N	6515.1	−2.1	187–656	260/40~ 100/1.7	12.13

Table 1. Cont.

Watershed Number	Name	Precipitation (mm)	Evaporation (mm)	Forest coverage (%)	Thickness of active layer (m)	R ²	E _{ns}
a	Emuer	460.4	886.6	76.6	0.3–1.0	0.79	0.81
	Pangu	463.2	881.1	75.3	0.4–1.2	0.76	0.73
b	Huma	483.5	905.7	70.7	0.4–1.8	0.83	0.85
c	Nuomin	480.2	1050	70.2	1.3–3.0	0.85–0.87	0.85
d	Taoer	435.4	1780	65.3	—	0.66–0.89	0.65–0.89
e	Hailaer	421.3	965.2	25.2	1.6–2.5	0.899	0.873
f	Hulun	285.6	1400.2	Typical grassland lake	—	0.875	0.94
g	Genhe	411.8	932.4	90.2	0.9–1.6	0.88	0.86
h	Jiliu	430.3	889.6	73.6	0.4–1.3	0.82	0.84
i	Kuerbin	617.4	930.7	73.9	1.4–1.8	0.79	0.83
j	Tangwang	627.9	805.0	80.3	1.4–1.8	0.83	0.87
k	Balan	616.3	1296.6	77.5	1.6–2.0	0.86	0.89
l	Xibei	610.0	1368.1	74.6	1.6–2.0	0.83	0.85
m	Chalin	615.5	1349.7	73.2	1.8–2.0	0.81	0.84
n	Hulan	576	1182.3	76.1	1.8–2.0	0.79	0.82
o	Numin	544.3	1238.8	78.3	1.6–2.0	0.85	0.86
p	Zhan	610.0	1388.2	77.1	1.4–1.8	0.85	0.88

Length (km)/Width (m)/Depth (m) of the rivers shown in the table is the length/width range/average depth of the corresponding river main stem in the list. The Annual Runoff (10^8 m^3) in the table is the runoff recorded at the control hydrological stations of the main streams of the rivers listed in the table, and the specific locations of the hydrological stations are shown in Figure 2. In addition, the Air Temp ($^{\circ}\text{C}$), Precipitation (mm), Evaporation (mm), Forest coverage (%) and Thickness of active layer (m) of each shown watershed are taken as the average value within the whole watershed corresponding to the years from 2000 to 2020. The values of R² and E_{ns} are the average of the calibrated data of each basin in the validation period. The value of active layer thickness is taken from permafrost-covered areas in the watershed, and areas without permafrost are not included in the calculation and statistics.

The following summarizes the sensitivity analysis of the hydrological parameters of the SWAT model in each basin. The groundwater supply in the permafrost region is mainly supplied by surface water, such as atmospheric precipitation, snowmelt and groundwater, and a large amount of water released from permafrost degradation is also one of the important water sources in the flood season of rivers in the permafrost region of Northeast China. After a long and stable negative temperature period, part of the permafrost seasonally melts, and the active layer deepens. The recharge sources of groundwater in the permafrost regions mainly include atmospheric precipitation, snowmelt water and the frozen layer melted into water in the warm season of the year. If the active layer is composed of rock layers with strong water permeability, such as the gravel layer and large gravel layer, atmospheric precipitation and surface water can also directly recharge deep groundwater. Moreover, as the terrain becomes more gentle and the vegetation density increases, the water supply efficiency of the groundwater released by permafrost melting also increases.

4. Discussion

The upper reaches of the watersheds in the studied permafrost area in Northeast China have large areas of primary forest, with high vegetation coverage and evapotranspiration, and are less affected by human activities. The permafrost layer shows a distribution pattern of thickness gradually becoming thinner from a high to low altitude, and from a high to low latitude, the thickness of the “active layer” changes oppositely. The part of precipitation that is not retained by leaves or vegetation and that is adsorbed by organic matter in the black earth layer on the surface enters the “active layer” through infiltration. The river runoff is not only related to precipitation and temperature but also closely related to the thickness of the active layer and the state of permafrost. In recent years, the temperature in the permafrost region of Northeast China has increased, resulting in increased evapotranspiration. In recent years, the temperature rise in the permafrost region in Northeast China has led to increased evapotranspiration, and the freezing process of the permafrost in Northeast China, taking the Greater Khingan Mountains region as an

example, has been delayed. In addition, the permafrost has degenerated and accelerated the release of water, affecting changes in runoff and other phenomena. According to the calculated thickness of permafrost after 100 years at a warming rate of $0.04\text{ }^{\circ}\text{C/a}$, the spatial distribution of permafrost ice storage in the current scenario shows that the ice storage of permafrost in China after 100 years decreases as the area of permafrost becomes smaller. The ice storage in all statistical intervals decreases significantly, and area with accumulated ice storage above 3m has basically disappeared. Only the higher latitude areas and the higher elevation areas, such as the Greater Khingan Mountains and the Changbai Mountains, still have permafrost deposits. The change in ice storage volume with elevation was calculated separately for each layer, and the change in ice storage volume with elevation after 100 years was obtained statistically (Figure 3f). There is some variability in the ice storage volume in terms of elevation. The ice content of permafrost is degraded in different elevation statistical areas, and lower elevation areas have a greater decrease in ice content compared to the higher elevation areas. The total ice storage volume reaches its maximum at around 1000 m, with a storage volume of about $343.35 \times 10^8\text{ m}^3$. Areas below 800 m in elevation no longer have permafrost deposits, and the average elevation of areas with permafrost deposits increases significantly. The comparative analysis shows that the total ice reserves in the permafrost region of Northeast China and the ice reserves at different altitudes and latitudes change greatly after 100 years. The calculated total ice storage volume is $3.178 \times 10^{11}\text{ m}^3$, and after 100 years, the storage volume becomes $6.641 \times 10^{10}\text{ m}^3$ with a decrease of $2.514 \times 10^{11}\text{ m}^3$. The water release volume accounts for 79.11% of the total storage volume, and the water release rate reaches $2.51 \times 10^9\text{ m}^3/\text{a}$. In the calculation of ice storage volume, the average water content of each layer of soil was used instead of the actual water content, which may have led to some deviations between the calculated value and the actual value, but the calculated ice storage volume still has some reference value.

1. The trends of monthly precipitation and runoff in each basin do not correspond exactly to each other. For example, in the Nuomin River Basin, the maximum precipitation and the maximum runoff do not occur in the same year; the maximum precipitation occurred in 2003, and the maximum runoff was in 2018 during the study period. To reveal the relationship between precipitation and runoff in the studied permafrost area, further analysis of precipitation and runoff distribution within basins from 2000 to 2020 (Figure 4a), as well as the fugacity state of permafrost in the basin, was carried out to infer three different types of runoff patterns due to different degrees of permafrost degradation in the permafrost area of Northeast China under the influence of climate, as shown in Figure 4b–d.
2. Surface runoff is mainly generated directly by precipitation in areas where permafrost is thick and the active layer thickness is thin, and the state of the permafrost deposit tends to be stable. Most of these permafrost areas in Northeast China are concentrated in the higher elevation ridges of the Greater and Lesser Khingan Mountains and the higher latitude regions of Northeast China. These areas tend to have lush vegetation coverage and are less affected by human activities, and precipitation is retained by the vegetation and then falls to the surface. Due to the small thickness of the active layer, the thick permafrost layer becomes impermeable to intercepting water, which affects the infiltration of water. When the amount of water infiltrated in the soil is greater than the maximum infiltration volume that can be achieved by the soil, which forms saturated excess runoff and forms a saturated thin layer in the unsaturated layer under the surface, the precipitation that cannot infiltrate into the “active layer” directly recharges the river through surface runoff.
3. The active layer is thicker in regions where permafrost degradation is more significant compared to stable permafrost regions. When the intensity of rainfall is less than the infiltration rate of the soil, it is difficult to form a saturated thin layer on the soil surface, and precipitation has little chance to form surface runoff. At this time, the precipitation infiltrates into the “active layer” on the permafrost to form a submerged

flow to recharge the river. Increasing river runoff from the submerged flow to recharge the river generally lags by 1–2 months. For example, in the Nuomin River Basin in July 2011, the highest precipitation for the year reached 197.4 mm, and the runoff in the Nuomin River Basin reached 213 m³/s in August, which was the maximum of the year. The maximum runoff lags behind the maximum precipitation by about 1 month, which indicates that the precipitation infiltrates into the “active layer” for about 1 month and then collects in the river water.

- At the edge of the degraded permafrost regions, such as the southern boundary of permafrost in Northeast China, where permafrost is extremely weak, water-resistant effects are extremely weak and have less influence on the infiltration process of water. The correspondence between runoff and precipitation as well as temperature in these areas is not significant. According to the principle of water balance, with the source of runoff recharge in the basin, in addition to the above-mentioned precipitation and permafrost water release, there is also pressurized water upwelling that recharges the river in addition to other ways. However, due to the amount of permafrost melting being low, evaporation and runoff in the basins are no longer significantly greater than the amount of precipitation.

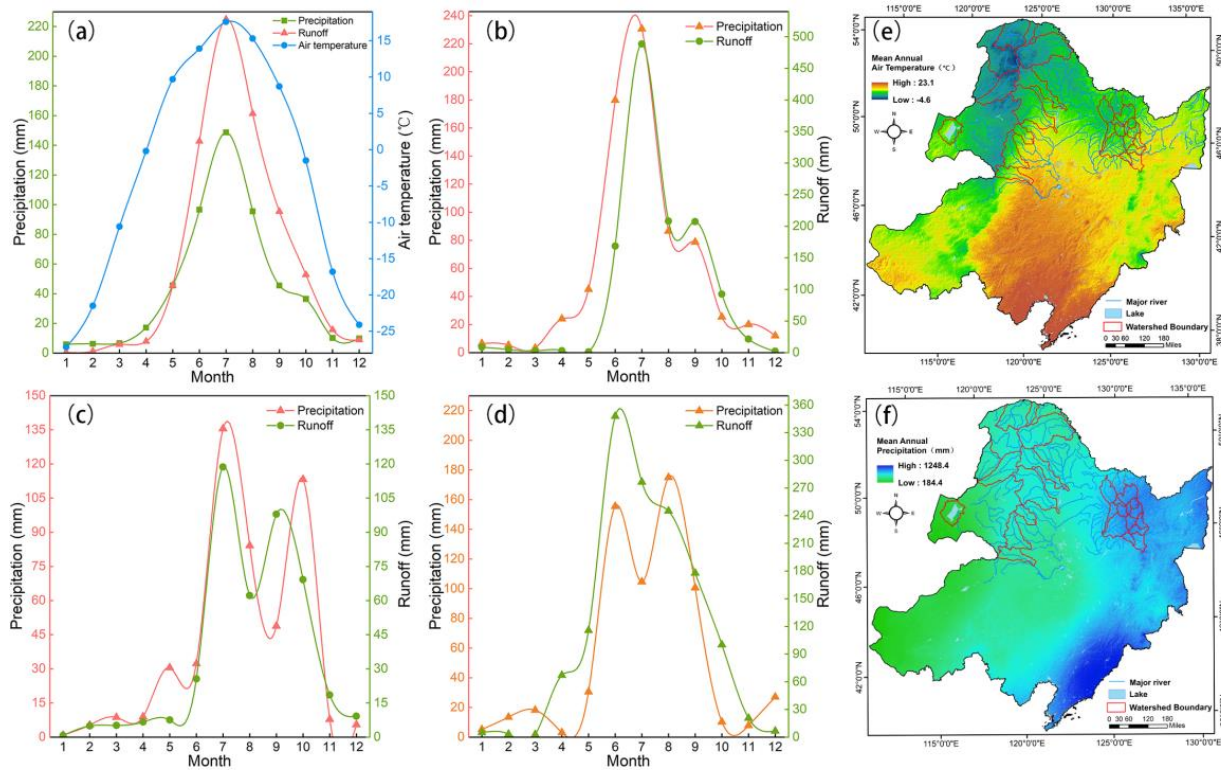


Figure 4. Diagram of the main runoff patterns under the influence of permafrost in Northeast China. (a) Monthly average precipitation, runoff and temperature for 2000–2020 for all watersheds studied; (b) Precipitation directly generates surface runoff; (c) Infiltration of precipitation into the “active layer” to form subsurface flow to recharge the river; (d) Upwelling of pressurized water to recharge rivers; (e) Distribution of the mean annual air temperature in watersheds of Northeast China; (f) Distribution of the mean annual precipitation in watersheds of Northeast China.

The flow production in the permafrost regions of Northeast China has obvious temporal characteristics during the year. From November to March each year, the average annual precipitation of the studied watersheds in the Northeast China permafrost regions is 30.1 mm, accounting for only 6.65% of the total average annual precipitation (452.6 mm), and most of the snowfall is concentrated in this period. The amount of water that can infiltrate into the “active layer” is very small, and the proportion of meltwater that recharges the

“active layer” via winter precipitation is low. Most of the permafrost regions in Northeast China have the climate conditions of rain and heat synchronization, and precipitation is concentrated from June to September when the average temperature is above 0°. The thawing of permafrost accompanied by concentrated precipitation causes a rapid increase in runoff and often causes flooding in many places. The melting of ice in the permafrost layer in each basin stops one after another in the middle and end of October, and the precipitation that enters the “active layer” after October is gradually frozen as the “active layer” becomes thinner and thinner if it does not flow out. After October, the runoff is mainly recharged by upstream rivers and lakes through lower unfrozen areas. The thermal effect of rivers on permafrost under the riverbeds is mostly manifested by the width of the thaw areas and the penetration, and the degree of the thermal effect varies depending on the size of the river and the water temperature. The spatial distribution of precipitation and air temperature in the watersheds located in the tundra of Northeast China is shown in Figure 4e–f. Many previous studies and explorations have shown that many of the larger rivers in Northeast China and rivers at lower latitudes in the regions have thorough thaw zones [59,60], and the effects of climate change on runoff have a lag effect, with the temperature of the previous period affecting the runoff of the next period and the growing season precipitation having a significant effect on the runoff of each period.

The distribution pattern of surface water in the Greater Khingan Mountains is from plains to hills and mountains, gradually increasing from south to north and increasing with permafrost and forest coverage. The total amount of surface water in the region is 37.096 billion m³ on average for many years, including 12 billion m³ in the Erguna River system and 18.4 billion m³ in the Nengjiang River system. The total area of the Greater Khingan Mountains is 31.08 million km², accounting for 26.8% of the total area of the region, and the river water resources account for 81.9% of the total amount of water in the region, which is the richest area of water resources in the whole region. In the northern part of the Greater Khingan Mountains, the forest coverage is larger, and the upper reaches of the Genhe and Kailu rivers located in the western part of the Greater Khingan Mountains are large areas of continuous permafrost compared with the island thaw area in the eastern part of the Greater Khingan Mountains and the Ganhe area in the island permafrost area, where the average annual precipitation is less and the runoff depth increases. In areas with higher precipitation in the eastern of the Greater Khingan Mountains, there are great differences in runoff depths due to different forest coverage and permafrost types.

The annual runoff of the river basin in the Lesser Khingan Mountains region in the last 20a shows a clear upward trend. The infiltration capacity of snowmelt water in the upper layer of the soil is enhanced during the melting period, and the unmelted layer of the permafrost located in the lower layer has a water-blocking effect. Therefore, the infiltration capacity of soil water is poor such that infiltrated water gathers in the relatively impermeable layer and forms runoff. One of the main factors affecting the hydrothermal properties of soil is soil temperature, and the change in soil temperature is a direct factor affecting the freezing and melting of soil water. In addition, precipitation is a major influential factor in the formation of runoff rainfall. In addition, runoff trends are consistent, and both show an increasing trend.

Permafrost has a direct impact on the conversion of rainfall into runoff correspondingly. Although the upper reaches of the Genhe and the Jiliu Rivers are not a high-value area in terms of annual precipitation, the flow-producing depth is the maximum in the Greater Khingan Mountains, with a total loss of about 200 mm, which is also the minimum loss in the Greater Khingan Mountains. The total loss in the southern part of the Greater Khingan Mountains is generally above 300 mm of maximum loss, and the flow-producing depth is generally between 50–75 mm. Huma River receives spring recharge in winter, and the water released from the permafrost layer through the transition of unfrozen areas in the permafrost layer recharges the river water. The sum of runoff and evapotranspiration in the Huma River Basin is greater than that of precipitation, further demonstrating that permafrost degradation releases a large amount of water to recharge rivers, increasing the

runoff in the study area. North of Genhe River is a large area of continuous permafrost that is many years old, and the thickness of the permafrost is 60–100 m. Every spring and summer, the temperature rises, and the surface can only be partly melted. The lower part is still permafrost, and an impermeable layer naturally forms. This layer is made from annual precipitation and partly from evaporation loss and the remaining water from the river flow. Therefore, this area is not a high-value precipitation area, but the runoff depth is the maximum in the Greater Khingan Mountains. Ganhe and Naduli Rivers belong to the island thawing area and island permafrost area. Except for the back shady slope part with permafrost and another sunny slope, most of the lower part of the riverbed does not have permafrost. The temperature and ground temperature are higher than those of the Genhe area, so the infiltration water and evaporation dissipation are more than those of the Genhe area. Therefore, the Ganhe and Naduli Rivers are high-value areas with an annual precipitation of 500 mm, but the runoff depth (210 mm) is not the maximum value of the Greater Khingan Mountains. The forest coverage in both regions is 75–80%, and the difference in flow production is caused by different types of permafrost. The seasonal permafrost area latitude is low, and the temperature and ground temperature are high. Permafrost thickness is greatly thinned, and there is no permafrost layer in the area, regardless of infiltration water or evaporation dissipation, which comprise a large area of continuous permafrost, island thaw area, island permafrost area and loss of water. Therefore, the precipitation into the runoff is lower. Compared with the Yalu River area, the forest coverage increases by about 30%, and the runoff increases by 60%. Compared with the Gan River and Naduri River, the forest coverage increases by about 110%. The runoff increases if compared with the Gen River and the upper reaches of the Jiliu River. The forest coverage increases by about 60%, and the annual precipitation is 5% less. However, the runoff depth increases by 15%.

The Greater Khingan Mountains permafrost region, which is located on the eastern side of the Hulun Lake Basin as the source of the Wursun River, is at the southern edge of the Eurasian continental permafrost belt, where the permafrost layer thickness is thin and its changes are extremely sensitive to temperature rises. Since the 1970s, the southern edge of the permafrost belt has shifted northward up to 30–100 km, and by 2000, the permafrost almost withdrew from the Hulun Lake Basin [27]. The meltwater runoff from the large-scale permafrost receding process in the basin directly recharged the river runoff and played a role in regulating the water conditions of the river and lake during the 1990s. The loss of meltwater recharge from the degradation of permafrost was also an important driving cause of the dramatic water condition changes in Hulun Lake after the 2000s.

5. Conclusions

Using field borehole data to simulate the permafrost fugacity in the permafrost regions of Northeast China during 2000–2020, combined with an analysis of climate and other hydrological environments of several major river basins in Northeast China, a distributed hydrological model was developed for several river basins during the study period. The effect of permafrost on runoff in Northeast China was analyzed, and the results of the study are summarized as follows.

(1) The thickness of permafrost in the permafrost regions of Northeast China increases with increasing altitudes and latitudes, as well as with decreasing mean annual ground temperature. The watershed on the western slope of the Great Khingan Mountains in the northernmost part of China covers an area of about 6.16×10^4 km² from the Tuli River northward to the Heilongjiang River. It is the region with the lowest temperature and greatest thickness of permafrost in Northeast China.

(2) The existence of permafrost forms a special runoff yield and concentration process, and it changes the water cycle process by affecting regional evapotranspiration and by reducing the soil infiltration rate and groundwater, among other factors, resulting in a certain intra-annual variation in runoff in the basin.

(3) In the context of global warming, the permafrost degradation and maximum freezing depth changes in the permafrost regions of Northeast China are accompanied by an increasing trend of annual runoff. The increase in precipitation is the main reason for the change in runoff volume, and the change in permafrost thaw depth affects the runoff yield and concentrating process, mainly by changing the soil water storage capacity. The effect of permafrost on small watersheds is more obvious, and the runoff in large watersheds shows more complex trends due to differences in snow storage, geomorphology, the existence of permafrost-free areas and other related factors.

(4) The main performance patterns of runoff changes in the watershed of the Northeast China permafrost regions are as follows: ① In early spring, the surface soil is in a frozen state, and there is nearly no surface runoff in the basin. Runoff is mainly recharged by groundwater. ② At the end of spring and the beginning of summer, in regions where permafrost is relatively stable and thick and where the active layer is thin, the depth of the thaw layer of the permafrost is still shallow. In addition, the existence of the permafrost layer is similar to an impermeable layer, which prevents the infiltration of snowmelt water, rapidly generates surface runoff and produces large flow per unit of area. Although the surface porous medium is frozen in spring, it can still allow some water to pass through, and the layer quickly generates runoff after it is full. ③ In summer, the maximum depth of the thaw layer is reached, and the permafrost layer is similar to the aquitard layer, which limits deep infiltration and increases the runoff coefficient, resulting in summer rainfall becoming the largest source of runoff recharge in permafrost regions. ④ In winter, springs and groundwater recharge the rivers, and the melting of river ice in spring also affects the hydrological process of meltwater runoff in permafrost regions. Snowmelt water in seasonal permafrost areas has a great contribution to groundwater recharge.

Author Contributions: Conceptualization, W.S.; data curation, Y.W. and Y.G.; formal analysis, C.Z.; funding acquisition, W.S.; methodology, S.L.; project administration, W.S. and L.Q.; software, Y.W.; supervision, W.S.; writing—original draft preparation, W.S., Y.W., Y.G. and C.Z.; writing—review and editing, W.S., Y.W., S.L., L.Q. and Y.G. All authors have read and agreed to the published version of the manuscript.

Funding: We thank the National Natural Science Foundation of China (Grant No. 41641024), the Carbon Neutrality Fund of Northeast Forestry University (CNF-NEFU) and the Science and Technology Project of Heilongjiang Communications Investment Group (Grant No. JT-100000-ZC-FW-2021-0182) for providing financial support and the Field Scientific Observation and Research Station of the Ministry of Education—Geological Environment System of Permafrost Areas in Northeast China (MEORS-PGSNEC).

Institutional Review Board Statement: Not applicable.

Informed Consent Statement: Not applicable.

Data Availability Statement: Related data are available upon reasonable request.

Conflicts of Interest: The authors declare no conflict of interest.

References

1. Guo, D.X. Some progress and existing problems of historical geocryology in China. *J. Glaciol. Geocryol.* **1988**, *3*, 300–303.
2. Xu, X.Z.; Wang, J.C.; Zhang, L.X. *Introduction Permafrost Physics*; Beijing Publishing House: Beijing, China, 2001.
3. Zhao, D.D.; Liu, J.F.; Liu, J.P.; Du, H.S. A review of main studies on permafrost degradation of Northeast China. *Sci. Technol. Eng.* **2002**, *22*, 13151–13161.
4. Liu, J.S.; Hayakawa, N.; Lu, M.J.; Dong, S.H.; Yuan, J.Y. Hydrological and Geocryological Response of Winter Streamflow to Climate Warming in Northeast China. *Cold Reg. Sci. Tech.* **2003**, *37*, 15–24. [[CrossRef](#)]
5. Walvoord, M.A.; Voss, C.I.; Wellman, T.P. Influence of permafrost distribution on groundwater flow in the context of climate-driven permafrost thaw: Example from Yukon Flats Basin, Alaska, United States: Permafrost distribution and groundwater flow. *Water Resour. Res.* **2012**, *48*. [[CrossRef](#)]
6. Chen, S.R.; Lv, S.H.; Kang, E.S.; Ji, X.B.; Yang, Y.; Zhang, J.S. A Distributed Water-Heat Coupled (DWHC) Model for Mountainous Watershed of An Inland River Basin (I): Model Structure and Equations. *Adv. Earth Sci.* **2006**, *21*, 806–818. [[CrossRef](#)]

7. Shen, Y.P.; Wang, G.Y. Key Findings and Assessment Results of IPCC WGI Fifth Assessment Report. *J. Glaciol. Geocryol.* **2013**, *35*, 1068–1076.
8. Zhang, L.; Guo, A.H.; Cao, Y.; Zhan, X.F. The characteristics of spatial-temporal changes in ground temperature at the depth of 0 cm in different regions across China during 1961–2020. *Chin. J. Ecol.* **2022**, 1–12. Available online: <https://xueshu.baidu.com/usercenter/paper/show?paperid=1v030e90at710rk0yb1104h0pj235313> (accessed on 22 November 2022).
9. Genxu, W.; Hongchang, H.; Taibin, L. The influence of freeze-thaw cycles of active soil layer on surface runoff in a permafrost watershed. *J. Hydrol.* **2009**, *375*, 438–449. [[CrossRef](#)]
10. Bense, V.F.; Ferguson, G.; Kooi, H. Evolution of shallow groundwater flow systems in areas of degrading permafrost. *Geophys. Res. Lett.* **2009**, *36*, L22401. [[CrossRef](#)]
11. St Jacques, J.-M.; Sauchyn, D.J. Increasing winter baseflow and mean annual streamflow from possible permafrost thawing in the Northwest Territories, Canada. *Geophys. Res. Lett.* **2009**, *36*, L01401. [[CrossRef](#)]
12. Lyon, S.W.; Destouni, G.; Giesler, R.; Humborg, C.; Morth, M.; Seibert, J.; Karlsson, J.; Troch, P.A. Estimation of permafrost thawing rates in a sub-arctic catchment using recession flow analysis. *Hydrol. Earth Syst. Sci.* **2009**, *13*, 595–604. [[CrossRef](#)]
13. McClelland, J.W.; Holmes, R.M.; Peterson, B.J.; Stieglitz, M. Increasing river discharge in the Eurasian Arctic: Consideration of dams, permafrost thaw, and fires as potential agents of change. *J. Geophys. Res. -Atmos.* **2004**, *109*, D18102. [[CrossRef](#)]
14. Li, X.; Cheng, G. A GIS-aided response model of high-altitude permafrost to global change. *Sci. China Ser. D-Earth Sci.* **1999**, *42*, 72–79. [[CrossRef](#)]
15. Nelson, F.E.; Outcalt, S.I. A Computational Method for Prediction and Regionalization of Permafrost. *Arct. Alp. Res.* **1987**, *19*, 279. [[CrossRef](#)]
16. Zhao, S.; Zhang, S.; Cheng, W.; Zhou, C. Model Simulation and Prediction of Decadal Mountain Permafrost Distribution Based on Remote Sensing Data in the Qilian Mountains from the 1990s to the 2040s. *Remote Sens.* **2019**, *11*, 183. [[CrossRef](#)]
17. Shi, Y.; Niu, F.; Yang, C.; Che, T.; Lin, Z.; Luo, J. Permafrost Presence/Absence Mapping of the Qinghai-Tibet Plateau Based on Multi-Source Remote Sensing Data. *Remote Sens.* **2018**, *10*, 309. [[CrossRef](#)]
18. Wang, K. A study on Simulation of the Permafrost Distribution on the Qinghai-Tibet Plateau Based on RS/GIS. Ph.D. Dissertation, Jilin University, Changchun, China, 2009.
19. Cheng, G.D. Exploration of the zonality pattern of permafrost at high altitude in China. *Acta Geogr. Sinica.* **1984**, *39*, 185–193. [[CrossRef](#)]
20. Li, X.; Cheng, G.D. Modeling the response of high-altitude permafrost to global change. *Sci. Sin. (Terrae)* **1999**, *29*, 185–192. [[CrossRef](#)]
21. Wu, Q.B.; Li, X.; Li, W.J. Computer Simulation and Mapping of the Regional Distribution of Permafrost along the Qinghai-Xizang Highway. *J. Glaciol. Geocryol.* **2000**, *22*, 323–326. [[CrossRef](#)]
22. Wu, Q.B.; Dong, F.X.; Liu, Y.Z. Spatial Distribution Model of High Ice Content Frozen Soil along Qinghai-Tibetan Highway—A GIS-aided model. *J. Glaciol. Geocryol.* **2004**, *26*, 137–141.
23. Qiu, G.Q.; Cheng, G.D. Permafrost in China—Past and Present. *Quat. Sci.* **1995**, *6*, 13–22+97.
24. Cheng, G.D.; Wang, S.L. On the zonation of high-altitude permafrost in China. *J. Glaciol. Geocryol.* **1982**, *2*, 1–17.
25. Nan, T.Z.; Li, S.X.; Liu, Y.Z. Mean Annual Ground Temperature Distribution on the Tibetan Plateau: Permafrost Distribution Mapping and Further Application. *J. Glaciol. Geocryol.* **2002**, *2*, 142–148.
26. Nan, Z.T.; Li, S.X.; Cheng, G.D.; Huang, P.P. Surface Frost Number Model and Its Application to the Tibetan Plateau. *J. Glaciol. Geocryol.* **2012**, *34*, 89–95.
27. Feng, Y.Q. Quantitative Analysis and Eco-Hydrology Effects of the Variation of Permafrost in the Qinghai-Tibetan Plateau. Master's Degree, China University of Geosciences, Beijing, China, 2015.
28. Bai, J.H. Multi-Model Analysis of Permafrost Changes in the Qinghai-Tibet Plateau and Its Hydrological Effects. Master's Degree, China University of Geosciences, Beijing, China, 2021. [[CrossRef](#)]
29. Lv, J.J.; Li, X.Z.; Hu, Y.M.; Wang, X.W.; Sun, J. Application of frozen number model in Northeast China Permafrost regionalization. *Chin. J. Appl. Ecol.* **2008**, *10*, 2271–2276.
30. Shan, W.; Zhang, C.; Guo, Y.; Qiu, L. Mapping the Thermal State of Permafrost in Northeast China Based on the Surface Frost Number Model. *Remote Sens.* **2022**, *14*, 3185. [[CrossRef](#)]
31. Frampton, A.; Painter, S.; Lyon, S.W.; Destouni, G. Non-isothermal, three-phase simulations of near-surface flows in a model permafrost system under seasonal variability and climate change. *J. Hydrol.* **2011**, *403*, 352–359. [[CrossRef](#)]
32. Sjöberg, Y.; Frampton, A.; Lyon, S.W. Using streamflow characteristics to explore permafrost thawing in northern Swedish catchments. *Hydrogeol. J.* **2013**, *21*, 121–131. [[CrossRef](#)]
33. Wang, S.C. Applicability study of runoff in North Cold Area Based on SWAT mode. *Pearl River* **2017**, *38*, 61–64. [[CrossRef](#)]
34. Evans, S.G.; Ge, S.; Liang, S. Analysis of groundwater flow in mountainous, headwater catchments with permafrost. *Water Resour. Res.* **2015**, *51*, 9564–9576. [[CrossRef](#)]
35. Qin, Y.; Yang, D.; Gao, B.; Wang, T.; Chen, J.; Chen, Y.; Wang, Y.; Zheng, G. Impacts of climate warming on the frozen ground and eco-hydrology in the Yellow River source region. *China. Sci. Total Environ.* **2017**, *605*, 830–841. [[CrossRef](#)]
36. Arnold, J.G.; Moriasi, D.N.; Gassman, P.W.; Abbaspour, K.C.; White, M.J.; Srinivasan, R.; Santhi, C.; Harmel, R.D.; van Griensven, A.; Van Liew, M.W.; et al. Swat: Model Use, Calibration, and Validation. *Trans. ASABE* **2012**, *55*, 1491–1508. [[CrossRef](#)]

37. Eckhardt, K.; Ulbrich, U. Potential impacts of climate change on groundwater recharge and streamflow in a central European low mountain range. *J. Hydrol.* **2003**, *284*, 244–252. [CrossRef]
38. Mango, L.M.; Melesse, A.M.; McClain, M.E.; Gann, D.; Setegn, S.G. Land use and climate change impacts on the hydrology of the upper Mara River Basin, Kenya: Results of a modeling study to support better resource management. *Hydrol. Earth Syst. Sci.* **2011**, *15*, 2245–2258. [CrossRef]
39. Wang, X.; Melesse, A.M. Evaluation of the SWAT model's snowmelt hydrology in a northwestern Minnesota watershed. *Trans. Asae* **2005**, *48*, 1359–1376. [CrossRef]
40. Tolson, B.A.; Shoemaker, C.A. Cannonsville Reservoir Watershed SWAT2000 model development, calibration, and validation. *J. Hydrol.* **2007**, *337*, 68–86. [CrossRef]
41. Meng, X.Y.; Shi, C.X.; Liu, S.Y.; Wang, H.; Lei, X.H.; Liu, Z.H.; Ji, X.N.; Cai, S.Y.; Zhao, Q.D. CMADS Dataset and its Application in Watershed Hydrological Simulation: A Case Study of the Heihe River Basin. *Pearl River* **2016**, *37*, 1–19. [CrossRef]
42. Shan, W.; Zhang, C.; Guo, Y.; Qiu, L.; Xu, Z.; Wang, Y. Spatial Distribution and Variation Characteristics of Permafrost Temperature in Northeast China. *Sustainability* **2022**, *14*, 8178. [CrossRef]
43. Liu, S.B.; Zang, S.Y.; Zhang, L.J.; Na, X.D. Estimation of land surface temperature from MODIS in Northeast China. *Geogr. Res.* **2017**, *36*, 2251–2260.
44. Luo, D.; Jin, H.; Jin, R.; Yang, X.; Lue, L. Spatiotemporal variations of climate warming in northern Northeast China as indicated by freezing and thawing indices. *Quat. Int.* **2014**, *349*, 187–195. [CrossRef]
45. Shi, S.; Li, W.; Ding, Y.S.; Lin, X.P.; Zhai, Y.C. Spatiotemporal evolution of vegetation and its response to climate change and human activities in Northeast China. *China Environ. Sci.* **2002**, *21*, 1–14. [CrossRef]
46. Liang, L.H.; Zhou, Y.W.; Wang, J.C. Changes of the Permafrost Environment in Great Xian Ridges after Disastrous Forest Fire: Taking Gulian Mining Area as an Example. *J. Glaciol. Geocryol.* **1991**, *13*, 17–25.
47. Ren, L.; Lin, Z.; Yong-Jian, D.; Ke-Qin, J.; Yin-Xue, W.; Yong-Ping, Q.; Er-Ji, D.; Guang-Yue, L.; Lin-Chan, S.; Yao, X. A study on soil thermodynamic characteristics of active layer in northern Tibetan Plateau. *Chin. J. Geophys.-Chin. Ed.* **2010**, *53*, 1060–1072. [CrossRef]
48. He, R.X.; Jin, H.J.; Zhao, S.P.; Deng, Y.S. Review of status and progress of the study in thermal conductivity of frozen soil. *J. Glaciol. Geocryol.* **2018**, *40*, 116–126.
49. Kersten, M.S. Laboratory research for the determination of the thermal properties of soils. *Univ. Minn. Minneap. Minn. Tech. Rep.* **1949**, *23*. Available online: <https://trid.trb.org/view/545019> (accessed on 22 November 2022).
50. Du, Y.S.; Li, R.; Wu, T.H.; Xie, C.W.; Xiao, Y.; Hu, G.J.; Wang, T.Y. Study of soil thermal conductivity: Research status and advances. *J. Glaciol. Geocryol.* **2015**, *37*, 1067–1074.
51. Chang, X.L.; Tie, L.M.; Jin, H.J.; He, R.X.; Li, X.Y.; Wang, Y.P. The features of permafrost in the Xinlin forest area on eastern slope of the Greater Khingan Mountains. *J. Glaciol. Geocryol.* **2015**, *42*, 823–833.
52. Zhao, L.; Ding, Y.J.; Liu, G.Y.; Wang, S.L.; Jin, H.J. Estimates of the Reserves of Ground Ice in Permafrost Regions on the Tibetan Plateau. *J. Glaciol. Geocryol.* **2010**, *32*, 1–9.
53. Xv, A.H. Analysis of the sensitivity of highway diseases in permafrost regions to ground temperatures and ice contents. *Arid. Land Geogr.* **2012**, *35*, 415–421.
54. Fu, S.H.; Wang, X.L.; Wang, H.Y.; Wei, X.; Yuan, A.P. Method of determining CN value in the SCS-CN method. *J. China Hydrol.* **2017**, *37*, 70–74.
55. Gu, W.; Li, L.; Shi, X.D.; Man, X.Y.; Shen, R.F. Application of Modified SCS Model in Runoff Simulation for Medium- and Small-sized Basins in Heilongjiang Province. *J. China Hydrol.* **2017**, *37*, 70–74.
56. Xiao, F.D.; Liao, H.C.; Guo, F. Water Resources and Sustainable Utilization in Cold Regions. In Proceedings of the Cold Region Water Science and International Rivers Research Series 2—Cold Region Water Cycle and Ice Engineering Research—Proceedings of the 2nd Symposium on Water Resources and Their Sustainable Use in Cold Regions, Heihe River, China, 25 July 2009.
57. Xiao, F.D.; Chen, P.Z. Rainfall-runoff relationship under the influence of frozen soil. *J. China Hydrol.* **1983**, *6*, 10–16. [CrossRef]
58. Zare, M.; Azam, S.; Sauchyn, D. A Modified SWAT Model to Simulate Soil Water Content and Soil Temperature in Cold Regions: A Case Study of the South Saskatchewan River Basin in Canada. *Sustainability* **2022**, *14*, 10804. [CrossRef]
59. Chen, J.S.; Wang, W.F.; Ma, F.Y. Recharge source and genesis analysis of Cenozoic basalt groundwater in Arshan. *J. Hohai Univ. Nat. Sci.* **2021**, *49*, 249–256.
60. Chang, Q.X.; Sun, Z.Y.; Ma, R.; Wang, X.; Long, X. A review of groundwater flow and its interaction with surface water in permafrost region. *Adv. Sci. Technol. Water Resour.* **2016**, *36*, 87–94.

Disclaimer/Publisher's Note: The statements, opinions and data contained in all publications are solely those of the individual author(s) and contributor(s) and not of MDPI and/or the editor(s). MDPI and/or the editor(s) disclaim responsibility for any injury to people or property resulting from any ideas, methods, instructions or products referred to in the content.